Electronic Supplementary Information (ESI)

Enhancing thermally activated delayed fluorescence characteristics by intramolecular B–N coordination in a phenylpyridine-containing donor–acceptor π-system

Kyohei Matsuo*[,†] and Takuma Yasuda*[,†,‡]

[†] INAMORI Frontier Research Center (IFRC), Kyushu University,
744 Motooka, Nishi-ku, Fukuoka 819-0395, Japan

[‡] Department of Applied Chemistry, Graduate School of Engineering,
Kyushu University, 744 Motooka, Nishi-ku, Fukuoka 819-0395, Japan

[*] E-mail: matsuo@ifrc.kyushu-u.ac.jp; yasuda@ifrc.kyushu-u.ac.jp

Table of Contents:

1. General

^{1}H and ^{13}C NMR spectra were recorded on a Bruker Avance III 400 spectrometer (400 MHz, for ^{1}H and 100 MHz for ^{13}C, respectively). Chemical shifts of ^{1}H and ^{13}C NMR signals were quoted to tetramethylsilane (δ = 0.00 ppm) and $CDCl_3$ (δ = 77.16 ppm) as internal standards. Matrix-assisted laser desorption ionization time-of-flight (MALDI-TOF) mass spectra were collected on a Bruker Daltonics Autoflex III spectrometer using dithranol as the matrix. Elemental analyses were carried out with a Yanaco MT-5 CHN corder. Single crystal X-ray diffraction measurement was performed on a Rigaku Saturn724+ diffractometer with multi-layer mirror monochromated Mo-Kα radiation at 123 K. The structures were solved by direct methods (SIR-2014[1]) and refined by the full-matrix least-squares on F^2 (SHELXL-2013[2]). All non-hydrogen atoms were refined anisotropically. All hydrogen atoms were placed using AFIX instructions. UV−vis absorption spectra were measured with a Jasco V-670 spectrometer. Fluorescence spectra were measured with a Jasco FP-8600 spectrophotometer. Absolute photoluminescence quantum yields (Φ_{PL}) were determined with a Jasco ILF-835 integrating sphere system. The transient PL characteristics were performed using a Quantaurus-Tau C11367 (λ_{ex} = 340 nm, pulse width = 100 ps, repetition rate = 20 Hz) under N_2 atmosphere, and a Hamamatsu Photonics C9300 streak camera with a N_2 gas laser (λ_{ex} = 337 nm, pulse width = 500 ps, and repetition rate = 20 Hz) under vacuum (< 4×10^{-1} Pa). The photoelectron yield spectra were measured with a Riken-Keiki AC-2 ultraviolet photoelectron spectrometer. All reactions were performed under a N_2 atmosphere. All regents and anhydrous solvents were purchased from Sigma-Aldrich, Tokyo Chemical Industry (TCI), or Wako Pure Chemical Industries, and were used without further purification unless otherwise indicated. 2-(4-Bromophenyl)pyridine (**3**)[3] and 2,7-dimethyl-10*H*-spiro[acridine-9,9´-fluorene] (**6**)[4] were prepared according to the literature procedure. OLED materials, 2,8-bis(diphenylphosphine oxide)dibenzo[*b*,*d*]furan (PPF)[5] and 9-phenyl-3,9'-bicarbazole (CCP)[6] were prepared by a procedure in the paper and then further purified by vacuum sublimation twice. 2,3,6,7,10,11-Hexacyano-1,4,5,8,9,12-hexaazatriphenylene (HAT-CN) was donated by the Nippon Soda Co., Ltd. and was purified by vacuum sublimation before use. Other OLED materials were purchased from E-Ray Optoelectronic Technology Co., Ltd. and were used without further purification. Final products **1** and **2** were purified by temperature-gradient sublimation to provide highly pure materials for optical property measurements and OLED device fabrications.

2. Synthesis

2-(4-Bromo-2-(dibrormoboryl)phenyl)pyridine (4): To a stirred solution of **3** (2.34 g 10.0 mmol) and diisopropylethylamine (1.9 mL, 11 mmol) in dry CH_2Cl_2 (70 mL) was added a heptane solution of BBr_3 (1.0 M, 30.0 mL, 30 mmol) at 0 °C. The mixture was stirred at room temperature for 24 h. The reaction was quenched by addition of saturated aqueous solution of K_2CO_3. The product was extracted with CH_2Cl_2. The combined organic layer was washed with water and brine, and dried over anhydrous Na_2SO_4. After filtration and evaporation, the crude product was washed with MeOH to afford **4** as a pale yellow solid (yield = 2.57 g, 64%). ^{1}H NMR (400 MHz, $CDCl_3$): δ 8.95 (d, J = 5.6 Hz, 1H), 8.19 (dd, J = 8.0, 8.0 Hz, 1H), 8.00 (s, 1H), 7.91 (d, J = 8.4 Hz, 1H), 7.63–7.55 (m, 3H). MS (MALDI-TOF): calcd for $C_{11}H_7BBr_2N$: 321.90 $[M-Br]^+$; found 321.80.

2-(4-Bromo-2-(diphenylboryl)phenyl)pyridine (5): To a stirred suspension of **4** (484 mg 1.20 mmol) and phenyltrimethylsilane (574 mg, 3.66 mmol) in *o*-dichlorobenzene (5 mL) was added $AlCl_3$ (17 mg, 0.13 mmol) at room temperature. The mixture was stirred at room temperature for 39 h. The reaction was quenched by addition of saturated aqueous solution of $NaHCO_3$. The product was extracted with CH_2Cl_2. The combined organic layer was washed with water and brine, and dried over anhydrous Na_2SO_4. After filtration and evaporation, the crude product was washed with MeOH to afford **5** as a white solid (yield = 267 mg, 56%). ^{1}H NMR (400 MHz, $CDCl_3$): δ 8.49 (dt, J = 5.6, 1.2 Hz, 1H), 8.07 (ddd, J = 8.0, 8.0, 1.6 Hz, 1H), 8.01 (dt, J = 8.0, 1.6 Hz, 1H), 7.83 (d, J = 1.6 Hz, 1H), 7.72 (d, J = 8.0 Hz, 1H), 7.46 (dd, J = 8.0, 2.0 Hz, 1H), 7.40 (ddd, J = 5.6, 5.6, 1.6 Hz, 1H), 7.21–7.17 (m, 10H). MS (MALDI-TOF): calcd for $C_{23}H_{17}BBrN$: 397.06 $[M]^+$; found 395.98.

10-(3-(Diphenylboryl)-4-(pyridine-2-yl)phenyl)-2,7-dimethyl-10*H*-spiro[acridine-9,9´-fluorene] (1): A mixture of **5** (239 mg, 0.600 mmol), **6** (259 mg, 0.721 mmol), $Pd_2(dba)_3$ (11 mg, 0.012 mmol), P(*t*-Bu)$_3$H·BF_4 (14 mg, 0.049 mmol), and sodium *tert*-butoxide (115 mg, 1.20 mmol) in dry toluene (6 mL) was stirred at 100 °C for 17 h under N_2. After addition of aqueous solution of NH_4Cl, the product was extracted with toluene. The combined organic layer was washed with brine and dried over anhydrous Na_2SO_4. After filtration and evaporation, the crude product was subjected to a silica gel column chromatography (eluent: hexane/toluene = 1:2, v/v). After removal of the solvents by evaporation, the resulting solid was recrystallized from $CHCl_3$/hexane solution to afford **1** as a yellow solid (yield = 181 mg, 45% yield). ^{1}H NMR (400 MHz, $CDCl_3$): δ 8.60 (d, J = 5.6 Hz, 1H), 8.17 (d, J = 8.0 Hz, 1H), 8.12 (d, J = 3.6 Hz, 2H), 7.88 (d, J = 1.6 Hz, 1H), 7.79 (d, J = 7.2 Hz, 2H), 7.48–7.40 (m, 4H),

7.36 (ddd, J = 8.0, 8.0, 1.2 Hz, 2H), 7.29–7.14 (m, 12H), 6.67 (dd, J = 8.4 Hz, 1.6 Hz, 2H), 6.35 (d, J = 8.4 Hz, 2H), 6.14 (d, J = 2.0 Hz, 2H), 1.92 (s, 6H). ^{13}C NMR (100 MHz, $CDCl_3$): δ 157.81, 156.82, 150.05, 144.65, 144.29, 140.89, 139.43, 139.36, 135.78, 133.97, 133.22, 129.41, 128.87, 128.55, 128.08, 127.96, 127.68, 127.51, 126.09, 126.00, 124.66, 124.29, 122.29, 119.87, 118.61, 114.81, 57.09, 20.51. MS (MALDI-TOF): calcd for $C_{50}H_{37}BN_2$: 676.30 $[M]^+$; found 676.34. Anal. calcd (%) for $C_{50}H_{37}BN_2$: C 88.75, H 5.51, N 4.14; found: C 88.87, H 5.52, N 4.13.

2,7-Dimethyl-10-(4-(pyridine-2-yl)phenyl)-10*H*-spiro[acridine-9,9´-fluorene] (2): A mixture of **3** (281 mg, 1.20 mmol), **6** (431 mg, 1.20 mmol), $Pd_2(dba)_3$ (22 mg, 0.024 mmol), P(*t*-Bu)$_3$H·BF_4 (28 mg, 0.096 mmol), and sodium *tert*-butoxide (231 mg, 2.40 mmol) in dry toluene (12 mL) was stirred at 100 °C for 17 h under N_2. After addition of aqueous solution of NH_4Cl, the product was extracted with toluene. The combined organic layer was washed with brine and dried over anhydrous Na_2SO_4. After filtration and evaporation, the crude product was subjected to a silica gel column chromatography (eluent: toluene). After removal of the solvents by evaporation, the resulting solid was recrystallized from $CHCl_3$/hexane solution to afford **2** as a white solid (yield = 519 mg, 84%). ^{1}H NMR (400 MHz, $CDCl_3$): δ 8.78 (d, J = 4.8 Hz, 1H), 8.31 (d, J = 8.0 Hz, 2H), 7.86 (m, 2H), 7.82 (d, J = 7.6 Hz, 2H), 7.59 (d, J = 8.4 Hz, 2H), 7.45 (d, J = 7.2 Hz, 2H), 7.39 (ddd, J = 8.0, 8.0, 1.2 Hz, 2H), 7.34–7.26 (m, 3H), 6.72 (dd, J = 8.4 Hz, 1.6 Hz, 2H), 6.34 (d, J = 8.0 Hz, 2H), 6.18 (d, J = 2.0 Hz, 2H), 1.95 (s, 6H). ^{13}C NMR (100 MHz, $CDCl_3$): δ 156.91, 156.70, 150.05, 142.51, 139.54, 139.43, 139.41, 137.09, 131.80, 129.69, 129.61, 128.51, 128.11, 128.03, 127.59, 126.00, 124.79, 122.62, 120.90, 119.96, 114.64, 57.09, 20.53. MS (MALDI-TOF): calcd for $C_{38}H_{28}BN_2$: 512.23 $[M]^+$; found 512.13. Anal. calcd (%) for $C_{38}H_{28}N_2$: C 89.03, H 5.51, N 5.46; found: C 89.24, H 5.47, N 5.44.

3. X-ray Crystallographic Analysis

Yellow block crystals of **1** were obtained by the recrystallization from ethyl acetate and acetonitrile using a vapor diffusion method. Total 21206 reflections were collected, among which 9218 reflections were independent (R_{int} = 0.0269). The crystal data: Formula $C_{54}H_{43}BN_4$; FW = 758.73, crystal size 0.19 × 0.10 × 0.06 mm, Monoclinic, $P2_1$ (#4), a = 8.898(5), b = 16.229(9), c = 14.316(8) Å, β = 95.661(7)°, V = 2057(2) Å^3, Z = 2, D_{calcd} = 1.225 g cm^{-3}, R_1 = 0.0382 ($I > 2\sigma(I)$), wR_2 = 0.0936 (all data), GOF = 1.070. Two acetonitrile molecules used as solvent were contained in asymmetric unit of crystal lattice, one of which was disordered. The crystal data is deposited in The Cambridge Crystallographic Data Centre (CCDC number: 1556338).

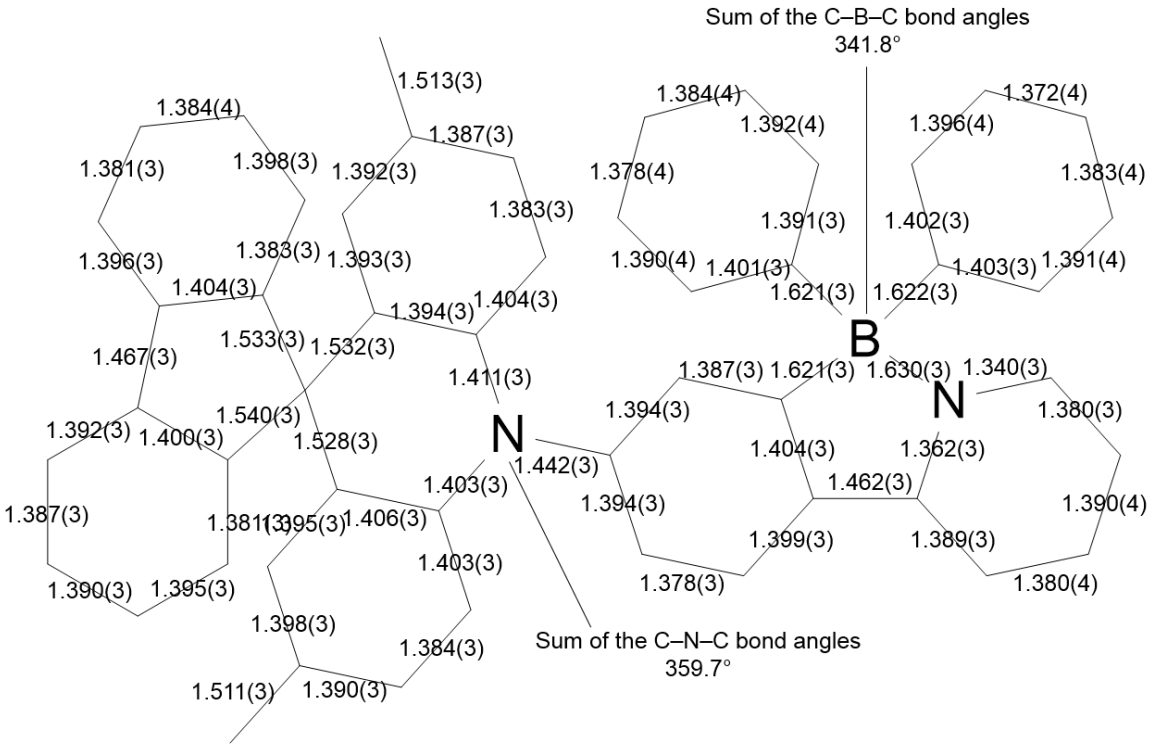

Fig. S1 Bond lengths (Å) of **1** in the X-ray crystal structure.

4. Computational Method

Geometry optimization in S_0 state of **1, 2**, and MFAc-PM were performed using the PBE0 functional with the 6-31G(d) basis set in the gas phase, implemented in the Gaussian 09 program package.[7] The Mulliken population analysis was applied to obtain the atomic contribution for the LUMO in the S_0 state. TD-DFT vertical excitation calculations were performed using the optimized geometry in S_0 state at the same level of theory. Geometry optimization in S_1 and T_1 states were performed using the optimized geometry in S_0 state as initial geometry with TD-DFT method at the same level of theory.

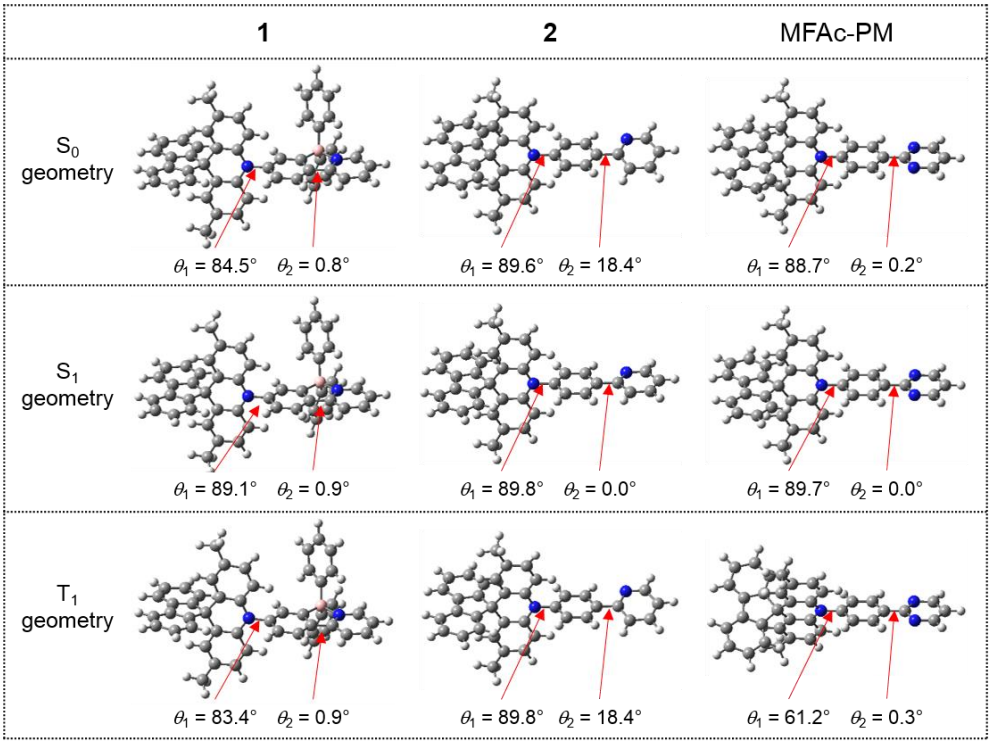

Fig. S2 Optimized structures of **1, 2** and MFAc-PM in S_0, S_1, and T_1 states at the PBE0/6-31G(d) level of theory. θ_1 is a torsion angle between acridan donor and phenylene ring. θ_2 is a torsion angle between the N-heteroarene ring and phenylene ring.

Table S1 TD-DFT Calculation Results S_1 and T_1 energies, oscillator strength (*f*), transition configurations, and singlet–triplet energy splittings (ΔE_{ST}) of the TADF molecules calculated at the PBE0/6-31G(d).

compound	state	*E* [eV]	*f*	main configuration [%]		ΔE_{ST} [meV]
1	S_1	2.134	0.0001	H → L	98	8
	T_1	2.126	0.0000	H → L	97	
2	S_1	2.715	0.0000	H → L	98	127
	T_1	2.588	0.0000	H−1 → L+2	90	
MFAc-PM	S_1	2.506	0.0000	H → L	99	130
	T_1	2.376	0.0000	H → L	70	
				H−6 → L	26	

H−*n* → L+*m* represents the HOMO−*n* to LUMO+*m* transition.

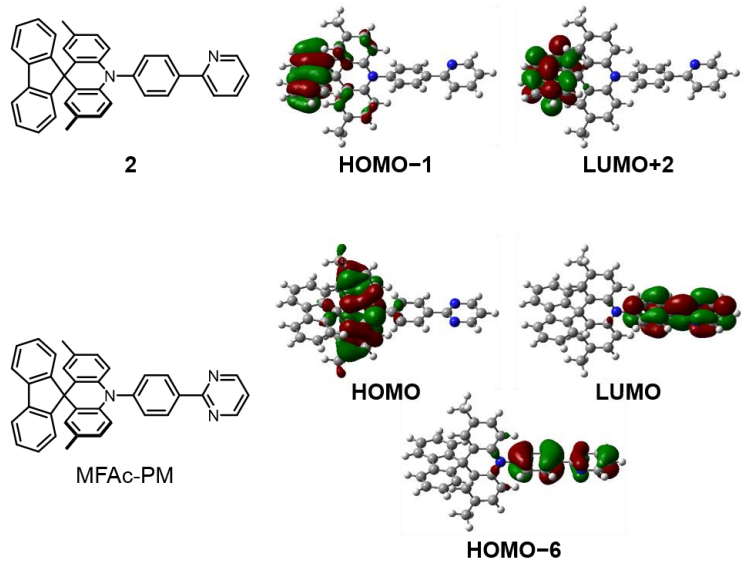

Fig. S3 Molecular orbital distributions of **2** and MFAc-PM.

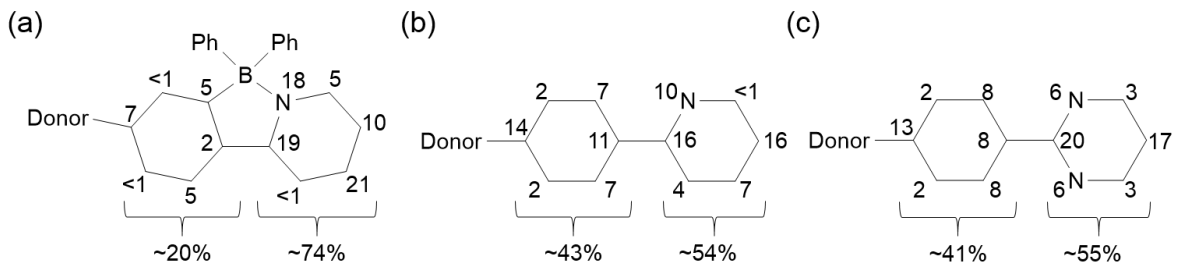

Fig. S4 Atomic orbital contributions (%) for the LUMOs of (a) **1**, (b) **2**, and (c) MFAc-PM.

5. Photophysical Properties

Photophysical properties of **1** and **2** in toluene solutions were measured by using deoxygenated spectral grade solvents in the concentration of 5×10^{-5} M.

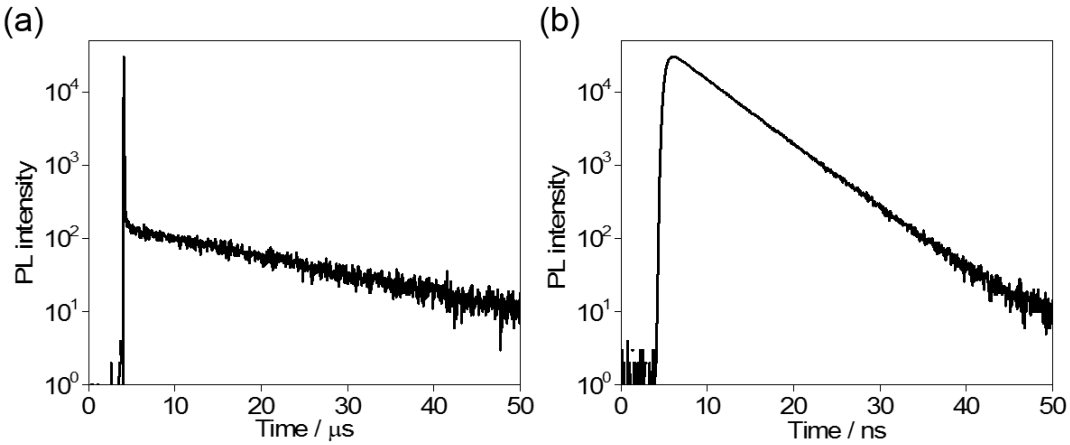

Fig. S5 Transient PL decays of (a) **1** and (b) **2** in deoxygenated toluene solutions at room temperature.

Table S2 Photophysical Data Measured in Toluene Solutions

	λ_{abs} [nm]	λ_{PL} [nm]	Φ_{PL} [%]	τ_p [ns]	τ_d [μs]
1	416	517	69	26	18
2	366	438	16	4.9	-

Pure neat films for the optical measurements were deposited under high vacuum ($< 1 \times 10^{-4}$ Pa) onto quartz or glass substrates, which were pre-cleaned by detergent, acetone, and isopropanol. The optical energy gaps (E_g) were determined from the high energy onset position of the UV-vis absorption spectra of pure neat films. The ionization potential (E_{IP}) were determined from the high energy onset position of the photoelectron yield spectra of pure neat films. The electron affinities (E_{EA}) were estimated by subtracting E_g from the measured E_{IP}.

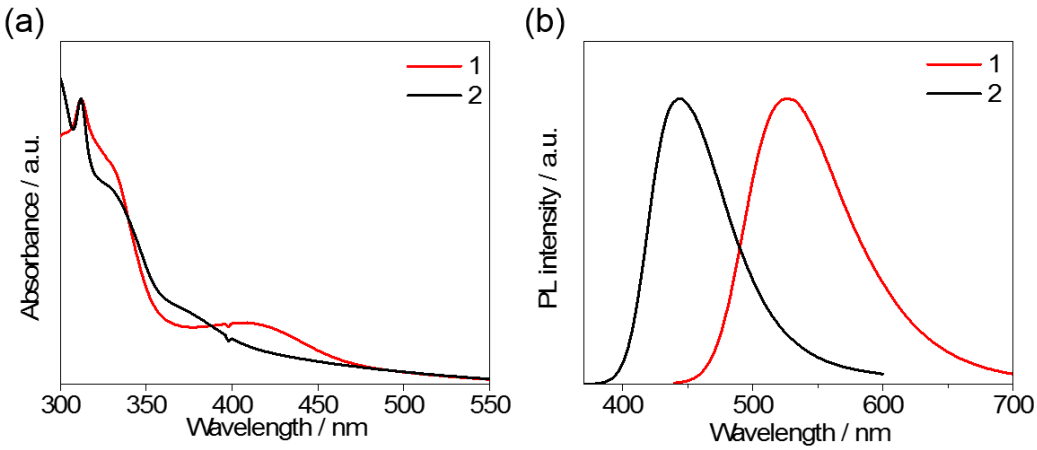

Fig. S6 (a) UV−vis and (b) PL spectra of **1** and **2** in pure neat films.

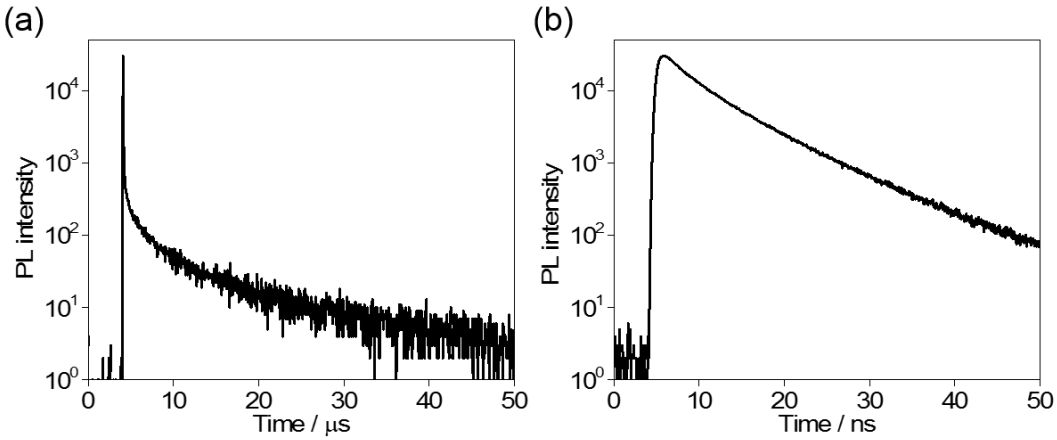

Fig. S7 Transient PL decays of (a) **1** and (b) **2** in pure neat films under N_2 atmosphere at room temperature.

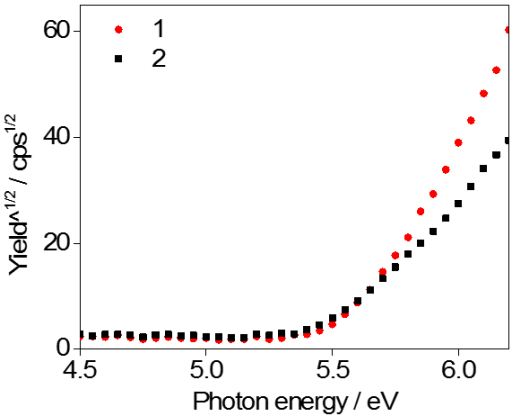

Fig. S8 Photoelectron yield spectra of **1** and **2** in pure neat films.

Table S3 Photophysical Data Measured in Pure Neat Films

	λ_{abs} (onset) [nm]	λ_{PL} [nm]	Φ_{PL} [%]	τ_p [ns]	τ_d [μs]	E_g [eV]	E_{IP} [eV]	E_{EA} [eV]
1	471	526	62	23	3.9	2.63	5.60	2.97
2	413	444	21	5.7	-	3.01	5.51	2.50

20wt%-doped films for the optical measurements were co-deposited with PPF as a host material under high vacuum (< 1×10^{-4} Pa) onto quartz substrates, which were pre-cleaned by detergent, acetone, and isopropanol. The singlet (E_S) and triplet excitation energies (E_T) were estimated from the high energy onset position of the fluorescence and phosphorescence spectra of 20wt%-doped films. The rate constants for the TADF decay process of **1** were calculated according to the literature.[8]

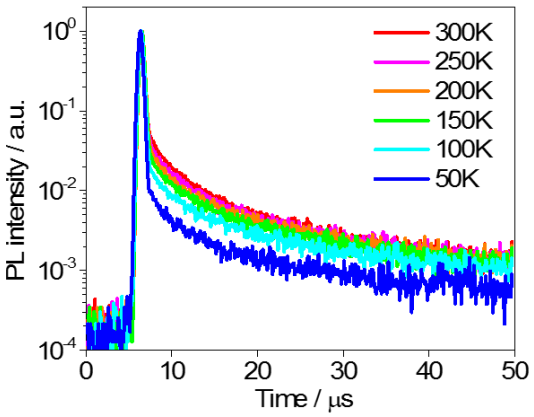

Fig. S9 Temperature dependence of transient PL decay of **1** ranging from 50 K to 300 K under vacuum.

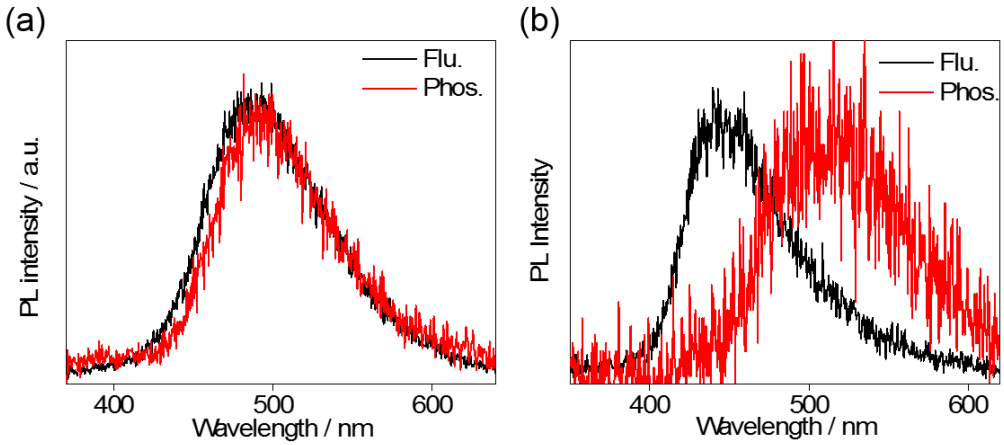

Fig. S10 Fluorescence (300 K) and phosphorescence (14 K) spectra of (a) **1** and (b) **2** in 20wt%-doped films under vacuum.

Table S4 Photophysical Data Measured in 20wt%-Doped Films in a PPF Host

	λ_{PL} [nm]	Φ_{PL} [%]	τ_p [ns]	τ_d [μs]	E_S [eV]	E_T [eV]	ΔE_{ST} [eV]
1	504	97	17	7.1	2.88	2.82	0.06
2	438	21	4.7	-	3.08	2.81	0.27
MFAc-PM[8]	466	91	13	45	3.06	2.80	0.26

Table S5 The Rate Constants and Quantum Efficiencies for Decay Processes in the 20wt%-Doped Films in a PPF Host

	k_r^S [10^7 s^{-1}]	k_{ISC} [10^7 s^{-1}]	k_{RISC} [10^5 s^{-1}]	Φ_p [%]	Φ_d [%]	Φ_{ISC} [%]	Φ_{RISC} [%]
1	2.7	3.1	2.8	47	50	53	94
2	4.5	-	-	21	-	-	-
MFAc-PM[8]	3.8	3.8	0.36	50	41	50	82

6. OLED Fabrication and Characterization

Indium tin oxide-coated glass substrates were cleaned with detergent, deionized water, acetone, and isopropanol. They were then treated with UV–ozone treatment for 30 min, before being loaded into a vacuum evaporation system. The organic layers were thermally evaporated on the substrates under vacuum (< 8×10^{-5} Pa) with an evaporation rate of < 2 Å/s. All of the layers were deposited through a shadow mask. The layer thickness and deposition rate were monitored *in situ* during deposition by an oscillating quartz thickness monitor. OLED properties were measured using a Keithley source meter 2400 and a Konica Minolita CS-2000.

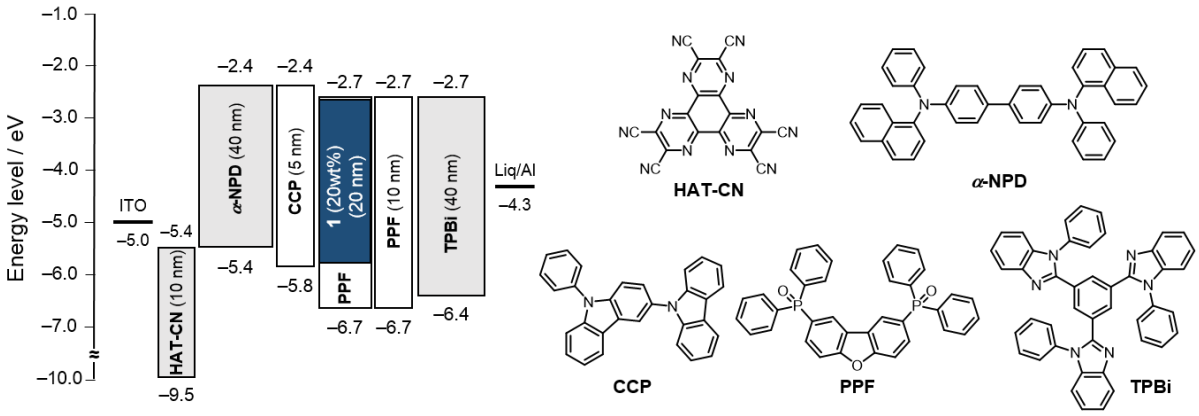

Fig. S11 Schematic energy-level diagram for OLED based on **1** as an emitter and molecular structures of the materials used in the devices.

Table S6 The EL Performance of the OLEDs based on 1.

	λ_{EL} [nm]	CIE (x, y)	V_{on} [V]	η_{ext} [%] Max / 10 / 100 cd m^{-2}	η_c [cd A^{-1}]	η_p [lm W^{-1}]
1	494	(0.20, 0.42)	3.8	22.7 / 22.3 / 14.1	56.4	44.3

[a]Abbreviations: λ_{EL} = EL emission maximum, CIE = Commission Internationale de l'Éclairage color coordinates, V_{on} = turn-on voltage at 1 cd m^{-2}, η_{ext} = maximum external EL quantum efficiency, η_c = maximum current efficiency, η_p = maximum power efficiency.

7. References

1. M. C. Burla, R. Caliandro, B. Carrozzini, G. L. Cascarano, C. Cuocci, C. Giacovazzo, M. Mallamo, A. Mazzone and G. Polidori, *J. Appl. Crystallogr.*, 2015, **48**, 306.

2. G. Sheldrick, *Acta Crystallogr., Sec. C*, 2015, **71**, 3.

3. J. Sun, H. Wang, H. Xu, T. Zhang, L. Li, J. Li, Y. Wu, B. Xu, X. Zhang and W. Lai, *Dyes Pigments*, 2016, **130**, 191.

4. I. S. Park, M. Numata, C. Adachi and T. Yasuda, *Bull. Chem. Soc. Jpn.*, 2016, **89**, 375.

5. P. A. Vecchi,A. B. Padmaperuma, H. Qiao, L. S. Sapochak and P. E. A. Burrows, *Org. Lett.*, 2006, **8**, 4211.

6. H. Wang, L. Xie, Q. Peng, L. Meng, Y. Wang, Y. Yi and P. Wang, *Adv. Mater.*, 2014, **26**, 5198.

7. Gaussian 09 (Revision C.01), M. J. Frisch, G. W. Trucks, H. B. Schlegel, G. E. Scuseria, M. A. Robb, J. R. Cheeseman, G. Scalmani, V. Barone, B. Mennucci, G. A. Petersson, H. Nakatsuji, M. Caricato, X. Li, H. P. Hratchian, A. F. Izmaylov, J. Bloino, G. Zheng, J. L. Sonnenberg, M. Hada, M. Ehara, K. Toyota, R. Fukuda, J. Hasegawa, M. Ishida, T. Nakajima, Y. Honda, O. Kitao, H. Nakai, T. Vreven, J. A. Montgomery, Jr., J. E. Peralta, F. Ogliaro, M. Bearpark, J. J. Heyd, E. Brothers, K. N. Kudin, V. N. Staroverov, T. Keith, R. Kobayashi, J. Normand, K. Raghavachari, A. Rendell, J. C. Burant, S. S. Iyengar, J. Tomasi, M. Cossi, N. Rega, J. M. Millam, M. Klene, J. E. Knox, J. B. Cross, V. Bakken, C. Adamo, J. Jaramillo, R. Gomperts, R. E. Stratmann, O. Yazyev, A. J. Austin, R. Cammi, C. Pomelli, J. W. Ochterski, R. L. Martin, K. Morokuma, V. G. Zakrzewski, G. A. Voth, P. Salvador, J. J. Dannenberg, S. Dapprich, A. D. Daniels, O. Farkas, J. B. Foresman, J. V. Ortiz, J. Cioslowski, and D. J. Fox, Gaussian, Inc., Wallingford CT, 2010.

8. I. S. Park, H. Komiyama and T. Yasuda, *Chem. Sci.*, 2017, **8**, 953.